Growth kinetics of intermetallic alloy phase at the interfaces of a Ni/Al multilayer using polarized neutron and x-ray reflectometry

Surendra Singh,[1] Saibal Basu,[1] M. Gupta,[2] C. F. Majkrzak,[3] and P. A. Kienzle[3]
[1]*Solid State Physics Division, Bhabha Atomic Research Center, Mumbai 400085, India*
[2]*UGC-DAE Consortium for Scientific Research, University Campus, Khandwa Road, Indore 452 017, India*
[3]*NIST Center for Neutron Research, National Institute of Standards and Technology, Gaithersburg, Maryland 20899, USA*
(Received 9 December 2009; revised manuscript received 8 February 2010; published 9 June 2010)

Al-Ni-based binary alloys offer several intermetallic phases of immense technological importance. We have attempted to understand the growth of interface alloy in an Al-Ni multilayer sample as a function of annealing time using primarily x-ray reflectometry (XRR) and polarized neutron reflectometry (PNR). Powder x-ray diffraction was also used to determine various crystallographic phases in the sample. The multilayer showed remarkable stability with respect to annealing time, following an initial alloy formation at the interface. Stability of such multilayers is important for their applicability as corrosion resistant coatings as well as metallization layers in microelectronic devices. Using XRR and PNR data we have identified the interface layer as Al_3Ni intermetallic phase. Magnetic depth profile obtained from PNR shows that the interface alloy layer is magnetically dead. From the Bragg peak intensities of polarized neutron reflectivity measurements, we have estimated the diffusion lengths after annealing at 160 °C for 1–8 h.

DOI: 10.1103/PhysRevB.81.235413 PACS number(s): 61.05.fj, 61.05.cm, 75.70.−i

I. INTRODUCTION

Intermetallic compounds consisting of a transition metal and aluminum are the subject of important industrial developments because of their high strength, hardness, high melting point, and resistance to oxidation along with favorable electronic and magnetic properties.[1–6] In addition, the intermetallic compounds in the form of thin-film structures play an important role in heat and corrosion resistant coatings or in metallization layers of microelectronic devices as well as in the areas of metallurgy and medicine.[1,7] The intermetallics of Al and Ni are the most studied ones because of their extremely desirable mechanical and thermal properties.[8] Ni and Al both have fcc structure at room temperature with cell parameters 3.52 Å and 4.05 Å, respectively, with Al having larger atomic radius. Al is soluble up to 20 % in Ni. Most importantly, apart from disordered solid solutions, Ni and Al form several ordered intermetallics. These are: Al_3Ni, Al_2Ni, Al_3Ni_2, AlNi, and $AlNi_3$ in order of increasing Ni concentration. The last one is of immense technological importance due to its large strength to weight ratio and high melting temperature. Stability of various intermetallic phases against thermal annealing is extremely important for their application. The alloy phases evolve from solid-state reactions at interfaces of their components. Multilayer samples are ideal for studying such reaction kinetics, since they provide a large number of interfaces. To understand the kinetics of alloy formation, one needs to characterize the interfaces during alloy formation in such multilayer samples. Rothhaar *et al.*[6] have studied phases formed after annealing of an Al/Ni stack with an average composition $Al_{0.5}Ni_{0.5}$, using Auger electron spectroscopy (AES) for depth profiling and x-ray diffraction (XRD). Depending on the temperature during annealing (between 160 and 330 °C for 45 min), they found that successively Al_3Ni, Al_3Ni_2, and then AlNi-ordered alloy phases formed. Since Ni is more mobile than Al due to its smaller atomic radius, such multilayers also show a large tail of Ni penetrating into Al layers. Some earlier works[9,10] focused on the interface properties of Ni/Al multilayers, using several techniques, viz., ion-beam depth profile, x-ray absorption spectroscopy, AES with sputtering depth profile, etc., which are limited in depth resolution. Some destructive techniques also cause relaxation and modification in the layers during sputtering, making physical interpretations more difficult. Neutron and x-ray reflectometry[11–15] are two nondestructive tools with depth sensitivity as low as 0.1 nm which allow one to examine the structure of thin films and multilayers with high depth resolution.

In this paper we present extensive polarized neutron and x-ray reflectivity measurements of Ni/Al multilayer samples that were grown by ion-beam sputtering and were annealed at 160 °C from 1 to 8 h under vacuum. X-ray reflectometry (XRR) and polarized neutron reflectometry (PNR) techniques were used to obtain depth-dependent chemical composition and magnetic-moment density in the sample, specifically targeting the composition of the interfaces. XRD was used to identify the crystalline structure of the interface alloy in the sample. While XRR depends on the electron-density profile in the layers, PNR depends on the nuclear coherent scattering length as well as the magnetic-scattering length density profile. This difference allows one to quantify the stoichiometry of the alloy at the interfaces, using the density profiles obtained from PNR and XRR, in case of binary alloys. In the present case we observed that the stoichiometry matches with the crystalline structure obtained from XRD. We find that the low-temperature anneal at 160 °C produced Al_3Ni-ordered phase at the interfaces as predicted by Bene's rule[16] and was also observed in an earlier work.[7] Most interestingly this ordered alloy phase produced a "*blocking effect*" at the moderate anneal temperature of 160 °C which inhibits further alloying at the interfaces, though the sample was annealed for 8 h at this temperature. We base our argument for such stability of the multilayer on thermodynamics of phase formation and the structure of the

interface alloy. We also show from PNR data that during the annealing process aluminum also penetrates the Ni layers, reducing the magnetic moment of Ni from 0.52 to 0.30 Bohr magneton (μ_B). The interface alloy layers in the present samples were magnetically dead.

II. SAMPLE PREPARATION AND EXPERIMENTAL TECHNIQUES

The Ni/Al multilayer sample was grown on Si substrate by ion-beam sputtering. In order to avoid contamination during deposition, the deposition system was thoroughly baked at a temperature of 200 °C for 12 h to achieve a background pressure of 2×10^{-9} Torr. Deposition of both Al and Ni layers was carried out at a rate of 0.1 Å/s. For the multilayer sample, first an Al layer of thickness ~50 Å was deposited on Si substrate followed by Ni layer of thickness ~50 Å. Ten such bilayers were deposited in the present case. During deposition, the thickness of each layer was monitored using a calibrated water-cooled quartz-crystal-thickness monitor. The as-deposited sample was characterized by PNR, XRR, and XRD. XRR and XRD data were collected on a laboratory x-ray source. The sample was annealed in steps for 1 h, 4 h, and 8 h under vacuum at a temperature of 160 °C. After each anneal PNR, XRR, and XRD data were collected on the sample.

The PNR data from as-deposited as well as annealed sample were obtained at the NG-1 reflectometer in NIST Center for Neutron Research (Gaithersburg, MD) using a neutron wavelength of 4.75 Å.[17] The scattering plane was horizontal, and the neutrons were polarized in the vertical direction, in the plane of the thin film, using supermirror polarizers. Typical polarization efficiencies exceeded 97%. The data were normalized and corrected for detector and polarizer efficiencies as described in Ref. 17. The reflectivity was measured as a function of wave-vector transfer Q [$=4\pi\sin(\theta)/\lambda$, where θ and λ are angle of incidence and wavelength of neutron, respectively] for both spin-flip (R^{+-} and R^{-+}, i.e., reflected neutrons with polarizations opposite to incident polarization), and nonspin-flip (R^{++} and R^{--}, i.e., reflected neutrons with the same polarization) settings. In case of R^{++}, the neutron spin polarization is parallel to the sample polarization and for R^{--} the neutron spin polarization is opposite to the sample polarization. The difference between two nonspin-flip cross-sections, R^{++} and R^{--}, is determined by the component of the magnetization parallel to the applied magnetic field (in-plane magnetization of sample). The remaining two spin-flip cross-sections, R^{+-} and R^{-+}, are related to the magnetization components perpendicular to the applied field. In all our data presented here, the spin-flip reflectivities were negligible, indicating that the magnetizations in the layers were collinear with the magnetic field (4.3 kG in the present case). The momentum transfer (Q) dependence of R^{++} and R^{--} profiles are related to the Fourier components of the magnetization depth profile, providing magnetic-moment density as a function of depth. The neutron reflectivity profile is usually fitted[15,18] using a model of the depth-dependent scattering length density (SLD) profile $\rho(z)$ (where z is the film depth) with nuclear and magnetic components

$$\rho(z) = \rho_{chem}(z) \pm \rho_{mag}(z); \quad \rho_{chem}(z) = \sum_i N_i(z) b_i;$$

$$\rho_{mag}(z) = C \sum_i N_i(z) \mu_i, \tag{1a}$$

where the summation is over each type of atom in the system, N is the in-plane average of the number density, b is the nuclear coherent scattering length, and μ is the magnetic moment in Bohr magnetons. The constant C is 2.69 fm/μ_B. The sign before ρ_{mag} in Eq. (1a) depends on the orientation of the magnetization relative to the neutron polarization. In the case of XRR the magnetic term is absent and the coherent scattering length "b" in Eq. (1a) is replaced by the Thomson scattering length for x rays, given by: $r_0(Z+f')$, where r_0 is the classical electron radius (2.8 fm), Z is the total number of electrons in the scattering atom, and f' is the dispersion term. The dispersion term is negligible at the x-ray energy considered here and the equation for x rays will be

$$\rho_{chem} = \sum_i N_i(z) r_0 Z_i. \tag{1b}$$

From both XRR and PNR, we obtain depth profiles of scattering length density in a sample. Since $N_i(z)$ the number density [Eqs. (1a) and (1b)] remains the same for XRR and PNR, in case of a multilayer with two elements, the value obtained for scattering length density $\rho(z)$ at the interfaces from PNR and XRR allows one to estimate the stoichiometry of the binary alloy at the interface quantitatively. For Ni and Al multilayers, the density of the alloy layer can be explicitly written in the form

$$\rho_{chem}^{neutron}(z) = N_{\mathrm{Al}}(z) b_{\mathrm{Al}} + N_{\mathrm{Ni}}(z) b_{\mathrm{Ni}};$$
$$\text{and} \quad \rho_{chem}^{x\ ray}(z) = N_{\mathrm{Al}}(z) r_0 Z_{\mathrm{Al}} + N_{\mathrm{Ni}}(z) r_0 Z_{\mathrm{Ni}}. \tag{2}$$

Equation (2) allows one to find out the stoichiometry of the interface layer from independent measurements of SLD using x-ray and neutron reflectometry. We had demonstrated earlier that from XRR and PNR data one could obtain stoichiometry of the alloy at the interface.[19] The present XRR data were collected on a Bruker's D8 advanced laboratory source.

Quantitative information on chemical and magnetic density profiles were extracted from the $\rho(z)$ model that reproduces the data with the lowest possible value of χ^2 using a Genetic algorithm,[20] which uses a matrix method[14] for generating the reflectivity pattern for a given set of physical parameters of the system.

III. RESULTS AND DISCUSSION

Figures 1(A) and 1(B) show XRD patterns recorded from an as-deposited Ni/Al multilayer and from the same Ni/Al multilayer annealed at 160 °C for 8 h, respectively. The XRD pattern changed after the first anneal for 1 h. In the subsequent anneals, the XRD pattern remained nearly unchanged up to an annealing time of 8 h. We have shown only

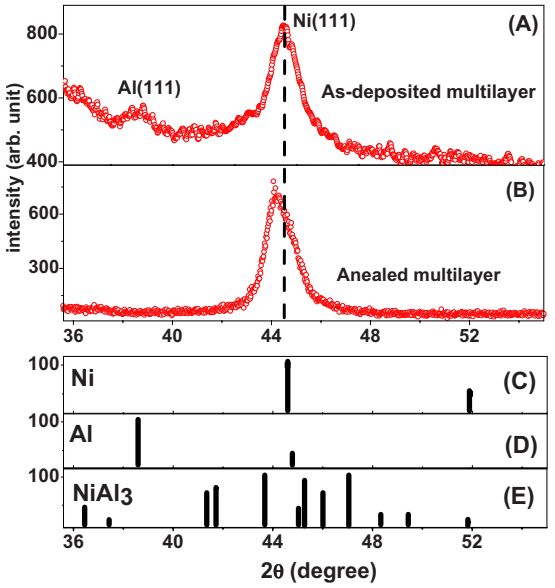

FIG. 1. (Color online) X-ray diffraction pattern of Ni/Al multilayer sample from (A) as-deposited, (B) after annealing at 160 °C for 8 h. The standard x-ray diffraction lines of (C) Ni, (D) Al, and (E) Al_3Ni.

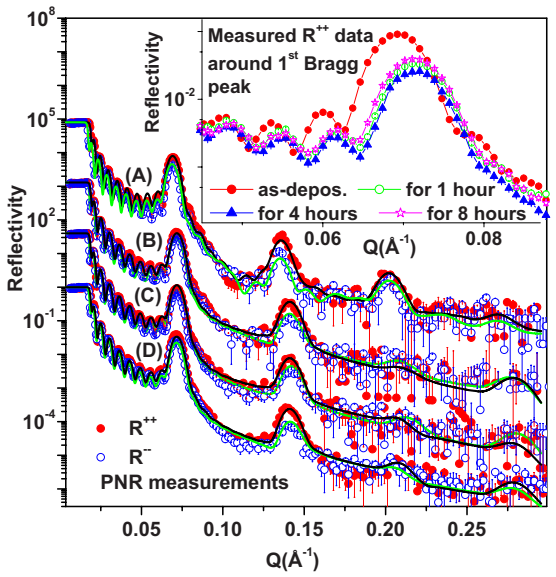

FIG. 2. (Color online) Measured NSF reflectivities R^{++} (solid circles) and R^{--} (open circles) for (A) as-deposited sample and sample annealed at 160 °C for (B) 1 h, (C) 4 h, and (D) 8 h, along with fits (solid lines) to the data from the corresponding scattering length density model (see text). The reflectivities of the as-deposited and annealed samples have been offset for better visualization. Inset shows the magnified version of measured NSF R^{++} data around first Bragg peak from as-deposited sample (closed circle), sample annealed at 160 °C for 1 h (open circle), 4 h (open triangle), and 8 h (open star).

the patterns corresponding to the as-deposited sample and the pattern after 8 h of annealing at 160 °C. The XRD pattern corresponding to the as-deposited multilayer sample [Fig. 1(A)] clearly shows two well-defined peaks at 2θ values of 38.4° and 44.5°. These peaks are due to the reflections from fcc Al (111) and fcc Ni (111), respectively. Only the Ni (111) diffraction peak with lattice spacing of $d_{\mathrm{Ni}(111)}$ =2.034 Å was observed for Ni in the multilayer that shows that the Ni layers had grown with a [111] texture along normal to the surface of the film. The XRD pattern confirmed that as-deposited Ni and Al layers were crystalline but textured along preferred direction. Often such multilayer samples with small layer thickness (~4–5 nm) grow with strong texture.[19,21] The broadening of the Ni [111] peak at 2θ=44.5° can be attributed to the effect of finite crystallite size limited to the thickness of Ni layers. In addition, the possibility of an Al (200) at 44.77° cannot be ruled out. We have shown the lines for fcc Ni, fcc Al, and ordered alloy Al_3Ni in Figs. 1(C)–1(E), respectively. In the annealed sample the peak due to Al has disappeared and a broad peak has appeared at a slightly lower angle (~0.27°) compared to the Ni [111] peak, which can be identified with Al_3Ni phase. Since there are a large number of possible Al_3Ni peaks as well as a possible Ni peak under this broad envelope, it is difficult to determine the nature of the interface alloy conclusively from XRD alone. It has been shown later from the scattering length density profiles obtained from XRR and PNR that the alloy phase has indeed the stoichiometry of Al_3Ni phase.

The two nonspin-flip (NSF) reflectivities R^{++} and R^{--} for the (A) as-deposited and annealed multilayer sample at 160 °C for (B) 1 h, (C) 4 h, and (D) 8 h are shown in Fig. 2, along with fits to the data generated from the corresponding SLD model. The reflectivities of both as-deposited and annealed multilayer samples have been offset for better visualization. The NSF reflectivity pattern from as-deposited sample clearly shows the presence of Bragg peaks up to fourth order. The Bragg reflection obtained in the NSF reflectivity pattern corresponds to a bilayer thickness of 91 Å with individual thicknesses of 47 and 44 Å for Ni and Al layers. The interface roughness for as-deposited Ni on Al was 8 Å and Al on Ni was 6 Å. The smaller oscillations (Kiessig oscillation) between the Bragg peaks, separated by $\Delta Q=2\pi/D$, due to the total multilayer thickness gives a total thickness $D\approx 900$ Å for the as-deposited sample. The sample was annealed for 1 h, 4 h, and 8 h, respectively. After each anneal of the sample PNR and XRR data were collected. All the Bragg peaks shift to marginally higher Q values after annealing, indicating small reduction in bilayer thickness. The inset of Fig. 2 shows the magnified version of the NSF (R^{++}) reflectivity pattern around first-order Bragg peak of as-deposited (closed circles) and samples annealed for 1 h (open circles), 4 h (open triangle), and 8 h (open star), to highlight the reduction in intensity as well as the shift in Bragg peak toward higher Q value on annealing. The small shift in the Bragg peaks we can only conjecture is due to defects getting annealed out. The reduction in the intensity of the Bragg peaks is due to alloying at the interfaces causing loss of contrast at the interfaces. It is clear from Fig. 2 and the inset that the modifications in the layer structure was largest after the first anneal, following which the structure did not change appreciably up to 8 h of annealing time. The nuclear (chemical) scattering length density (ρ_{chem}) model used to successfully fit the data are shown in Fig. 3 for (A)

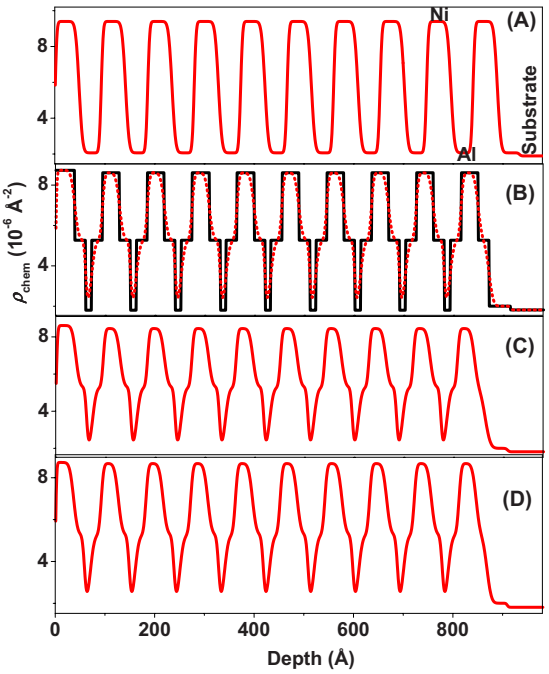

FIG. 3. (Color online) The chemical (nuclear) SLD models for (A) as-deposited Ni/Al multilayer samples as well as the sample annealed at 160 °C for (B) 1 h, (C) 4 h, and (D) 8 h from the fits to the NSF PNR reflectivity data. The solid line in (B) is the model for the density profile in absence of any interface roughness, which has been plotted for better visualization of interfaces.

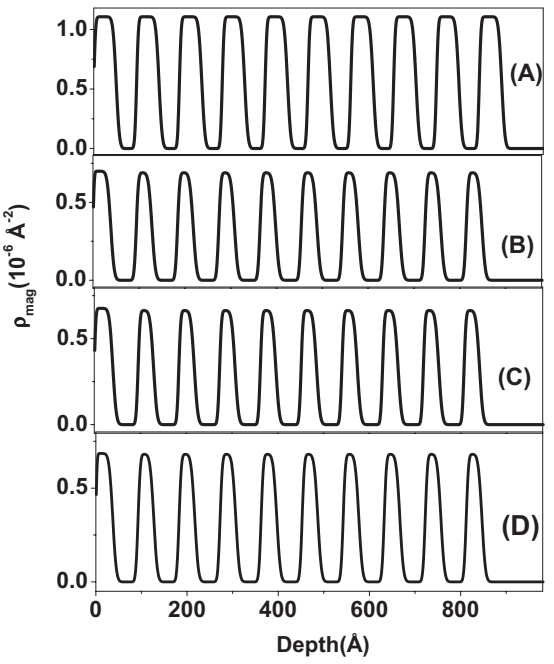

FIG. 4. The magnetic-scattering length density profile from fits to the polarized neutron reflectometry data (R^{++} and R^{--}) for (A) the as-deposited sample and the sample annealed at 160 °C for (B) 1 h, (C) 4 h, and (D) 8 h.

as-deposited and annealed samples at 160 °C for (B) 1 h, (C) 4 h, and (D) 8 h, respectively. The best-fit $\rho(z)$ model for the as-deposited sample shows that the ρ_{chem} values for Ni and Al layers are 9.35×10^{-6} Å^{-2} and 2.01×10^{-6} Å^{-2}, respectively, close to their natural bulk values. In Fig. 3(B) the solid line is SLD profile from the sample annealed at 160 °C for 1 h considering zero interface roughness, used as a guide to the eyes for visualization of the interface alloy layer between Ni and Al layers. The dashed line in Fig. 3(B) is the chemical SLD after including the effect of interface roughness due to alloying as represented by an error function at the interfaces. After annealing the sample at 160 °C for 1 h, the individual layer thicknesses of Ni (35 Å) and Al (12 Å) have substantially reduced from the as-deposited values of 47 Å and 44 Å, respectively. An interface layer has grown at their cost. We obtain an interface layer thickness of 22 Å. The interface alloy layer has a SLD $\rho_{chem}=5.20\times10^{-6}$ Å^{-2}. On further annealing the sample up to 8 h at the same temperature (160 °C) we did not find any major changes in the structural parameters obtained from NSF reflectivity data. The magnetic SLD (ρ_{mag}) models for best fit of the NSF reflectivity data from the as-deposited sample and the sample annealed at 160 °C for 1 h, 4 h, and 8 h are shown in Figs. 4(A)–4(D), respectively. The ρ_{mag} for each Ni layer for the as-deposited sample is 1.10×10^{-6} Å^{-2} giving approximately 0.52 μ_B per Ni atom, marginally less than its bulk value (~0.56 μ_B). The reduction in Ni layer thickness on annealing is coupled with further reduction in magnetic moment of the Ni atom to 0.30 μ_B per Ni atom. The alloy layer at the interfaces shows zero magnetic moment. There are first principle calculations on Ni films,[22] which show a reduction in magnetic moment of the Ni atom from 0.56 to 0.25 μ_B on reducing the nearest neighbor from 4 to 1. In the present case we can attribute this reduction to loss of Ni neighbors due to interface alloying and partially to diffusion of Al in the Ni layer. We later attempt to estimate this diffusion length from reduction in the intensity of Bragg peaks in PNR on annealing.

The XRR data are plotted as a function of momentum transfer Q for the as-deposited sample (closed circles) and the sample annealed at 160 °C for 8 h (open circles) in Fig. 5. We have also shown in the inset of Fig. 5, the XRR data up to 0.1 Å^{-1} for the sample annealed for 1 h, 4 h, and 8 h to highlight that after the first anneal there is no further change in the reflectivity. To obtain the structural parameters of the multilayers, we have fitted the XRR data to an electron SLD model taking into account the real and the imaginary parts of the scattering length, where the latter is related to absorption. Open and closed circles in Fig. 5 are experimental data whereas the solid lines are fit to measured data using a complex SLD model. The real part of the fitted SLD for the as-deposited and the annealed samples is shown in Figs. 6(A) and 6(B), respectively. In case of the as-deposited sample the Bragg reflections occur at $Q=2\pi n/d_{bl}$, where n is an integer and $d_{bl}\approx90$ Å is bilayer thickness. Bragg peaks up to fifth order due to the bilayer periodicity are seen in the as-deposited film. XRR data from as-deposited multilayer gave individual thicknesses of 49 Å and 41 Å for Ni and Al layers, respectively. The thickness of the Ni and Al layers for the XRR data are marginally different from the values obtained from PNR fits. One can see from Fig. 5 that the higher order Bragg peaks in XRR have also reduced in intensity

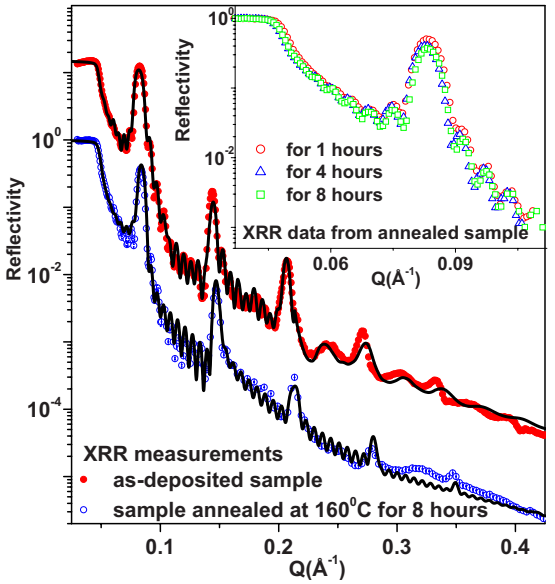

FIG. 5. (Color online) XRR pattern for as-deposited Ni/Al multilayer sample (closed circles) and sample annealed at 160 °C for 8 h (open circles). Continuous lines are fits to data. Inset shows the measured XRR data from sample annealed at 160 °C for 1 h (open circles), 4 h (open triangles), and 8 h (open rectangles) to highlight stability of the XRR pattern against annealing.

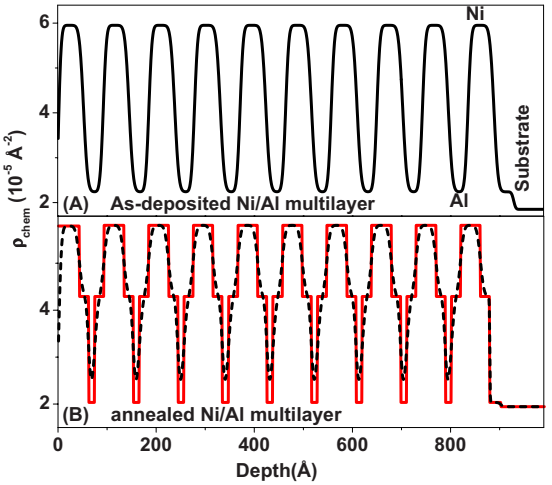

FIG. 6. (Color online) The chemical scattering length density profile for (A) as-deposited and (B) annealed sample at 160 °C for 8 h as obtained from measured XRR data. The solid line in (B) is the model for the density profile in absence of any interface roughness.

after annealing due to alloy formation at the interface. The alloy phase, which formed at the interface during the first anneal, inhibited further alloying.

For the as-deposited sample the fitted density profile [SLD profile in Fig. 6(A)] shows Ni and Al layers with reasonably sharp interfaces, which correspond to the solid line in Fig. 6(A). The fitted SLD for XRR data from the sample after annealing clearly shows an intermediate alloy layer sandwiched between Ni and Al layers [Fig. 6(B)]. The solid line is the histogram of SLD from the best fit and the dashed line in the same figure is an error function, representing a continuous change in density to model the interface roughness. Since the XRR pattern also does not change appreciably after the first anneal, we showed data and fits along with the corresponding SLD profiles only for the as-deposited sample and from the same sample after annealing it for 8 h, in Fig. 6. Fits show that on annealing at 160 °C the individual Ni and Al layer thicknesses have substantially reduced from original values of 49 Å and 41 Å to 34 Å and 12 Å, respectively, and an interface alloy layer of thickness ~20 Å has formed in this process. These thickness parameters are close to the value we obtained from PNR measurements. The excellent match between physical parameters obtained from the NSF, PNR profile, and XRR profile for the as-deposited sample and the sample annealed at 160 °C is evident in Table I. We also observe that the Bragg peaks in the XRR pattern also systematically shifted toward higher Q values, similar to the PNR data, presumably due to defects getting annealed out. The average scattering length density of the interface layer, as obtained from XRR measurements for the annealed sample is 4.30×10^{-5} Å^{-2}. To quantify the composition of the interface layer we have used XRR and PNR data together as shown in Eq. (2). Using the ρ_{chem} values obtained from XRR and PNR we obtained the stoichiometry of the interface alloy layer, Al:Ni ratio, 2.9:1, identifying the interface phase as Al_3Ni.

TABLE I. Physical parameters obtained from PNR and XRR measurements of as-deposited sample and sample annealed at 160 °C. The errors on the parameters are less than 5%.

	Parameters [d=thickness(Å), ρ_{chem}=nuclear-scattering length density (10^{-6} Å^{-2}), and σ=roughness(Å)] extracted from PNR measurements						Parameters [d=thickness(Å), ρ_{chem}=electron-scattering length density (10^{-5} Å^{-2}), and σ=roughness(Å)] extracted from XRR measurements					
	As deposited			Annealed			As deposited			Annealed		
Layer	d	ρ_{chem}	σ	d	ρ_{chem}	σ	d	ρ_{chem}	σ	d	ρ_{chem}	σ
Alloy				22	5.17	3				20	4.30	3
Ni	47	9.35	6	35	8.68	7	49	5.95	7	34	5. 8	6
Alloy				22	5.17	3				20	4.30	3
Al	44	2.01	7	12	1.80	7	41	2.24	7	12	2.1	7
Subs.		1.84	5		1.83	5		1.94	5		1.93	5

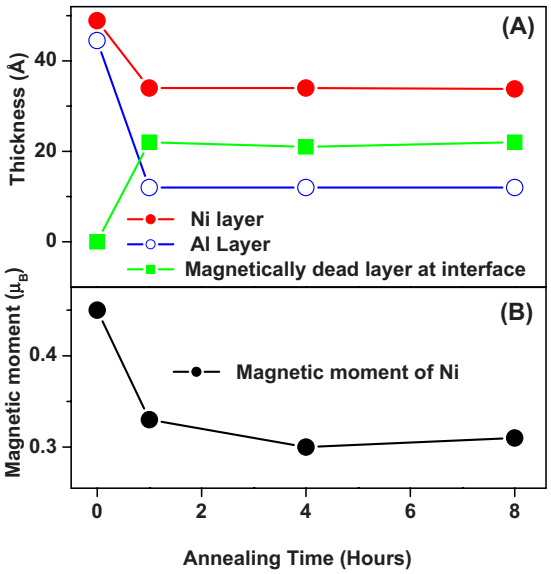

FIG. 7. (Color online) (A) Thickness variation in individual Ni layer (closed circles), Al layer (open circles), and alloy layer (closed squares) as a function of annealing time. (B) The average magnetic moment of Ni atom in individual Ni layer (closed circles) as a function of annealing time.

We observe that though the sample was annealed only at 160 °C, there was rapid alloying at the interfaces during first 1 h of annealing, evident from XRD, PNR, and XRR data. The remarkable stability of the multilayer film following the first anneal is the most important observation in the present set of studies supported by XRD, PNR as well as XRR data. The results have been consolidated in Figs. 7(A) and 7(B), in which we have combined the plots of thickness of the alloy layer (magnetically dead), thickness of Al and Ni layers and the magnetic moment in the Ni layers as functions of annealing time. This plot highlights the observation that following the first anneal, the multilayer showed remarkable stability against further annealing. In addition PNR measurements also show that the alloy layers at the interfaces are magnetically dead and that there is a large reduction in magnetic moment in the Ni layers due to diffusion of Al into the Ni layer.

Another important parameter which could be quantified from PNR and XRR reflectivity data is the diffusivity of the constituent elements at the interfaces. The observed decay of Bragg peak intensity in PNR measurements from the sample annealed at 160 °C for 1–8 h could be used to calculate the diffusivity of the constituent element as well as the interdiffusion length at this annealing temperature using the expression[23]

$$\ln[I(t)/I(0)] = -8\pi^2 n^2 D(T) t/d_{\mathrm{bl}}^2, \tag{3}$$

where $I(0)$ is the intensity of the nth order Bragg peak at time $t=0$, D is the diffusivity at the annealing temperature T, and d_{bl} is the bilayer periodicity. The average diffusion length L_d is related to the diffusivity $D(T)$, through the relation: $L_d=\sqrt{6D(T)t}$, where t is the annealing time. The Bragg intensity for first-order peak (inset of Fig. 2) was determined after subtracting the background due to Fresnel reflectivity. We obtained a diffusion length of approximately 23.5 Å after the sample was annealed at 160 °C for 1 h, which remained almost constant with time. The diffusion length obtained from this measurement is close to the thickness of alloy layer at interfaces as obtained by XRR and PNR measurements.

In the present case the low-temperature anneal at 160 °C produced an Al_3Ni phase at the interface conforming to the rule that in case of metal-metal nucleation, the first phase that forms is the one adjacent to the low-temperature eutectic in the binary phase diagram.[16] This observation is also in line with earlier work by Rothhaar *et al.*[6] Once Al_3Ni phase forms at the interface, the stability of the multilayer against further annealing may be attributed to the thermodynamics of phase formation and structure of the interface alloy. Ni and Al both are fcc metals. When mixed to form binary alloys they form Ni_3Al and Al_3Ni at two ends of the phase diagram; the former is the high-temperature eutectic and the later is the low-temperature eutectic. While Ni_3Al has an ordered fcc phase, Al_3Ni is orthorhombic. Both have A_3B-type coordination, where each A atom is surrounded by 12 B atoms and vice versa. These structures have the largest number of nearest neighbors among all the metallic lattices. From the point of view of energy, A-B bonds are preferred to A-A or B-B type of bonds. This will reflect in the free energy "F" for the system, given by U-TS (U, T, and S are internal energy, temperature, and entropy, respectively), where the bond energy gives the internal-energy part "U." Since we have annealed at a comparatively low temperature, the entropy term cannot override the internal energy to cause any fluctuation in the composition necessary for mixing and diffusion, leaving a stable multilayer. Also the interface alloy Al_3Ni in this case is an orthorhombic phase and does not have the directional symmetry of a cubic fcc phase. In case the interface alloy grows with some preferred orientation, that might cause anisotropic diffusion with a low-diffusion constant normal to the planes of the multilayer.

IV. SUMMARY AND CONCLUSIONS

To summarize, we have characterized the kinetics of alloy formation in a Ni/Al multilayer by annealing the sample at 160 °C. The as-deposited sample and the annealed sample were characterized using x-ray diffraction, polarized neutron reflectometry, and x-ray reflectometry. We observed that initially the Al_3Ni phase formed as the interface alloy layer in the multilayer sample. The sample showed remarkable stability against any further annealing at this temperature. The layered structure remained almost the same up to 8 h of annealing time. This has been confirmed from all three measurements independently. PNR showed that the interface alloy layer was magnetically dead and the magnetic moment in the Ni layer reduced from 0.52 to 0.30 μ_B per Ni atom due to Al diffusion into the Ni layers.

[1] D. B. Fraser, in *VLSI Technology*, edited by S. M. Sze (McGraw-Hill, New York, 1983), p. 347.
[2] M. Wittmer, J. Vac. Sci. Technol. A **2**, 273 (1984).
[3] E. Besnoin, S. Cerutti, O. M. Knio, and T. P. Weihs, J. Appl. Phys. **92**, 5474 (2002).
[4] R. Darolia, D. F. Lahrman, R. D. Field, J. R. Dobbs, K. M. Chang, E. H. Goldman, and D. G. Konitzer, in *Ordered Intermetallics-Physical Metallurgy and Mechanical Behavior*, edited by C. T. Liu, R. W. Cahn, and G. Sauthoff (Kluwer Academic, Dordrecht, 1992), p. 679.
[5] E. P. Busso and F. A. Mcclintock, Acta Metall. Mater. **42**, 3263 (1994).
[6] U. Rothhaar, H. Oechsner, M. Scheib, and R. Müller, Phys. Rev. B **61**, 974 (2000).
[7] E. G. Colgan, Mater. Sci. Rep. **5**, 1 (1990).
[8] A. I. Taub and R. L. Fleischer, Science **243**, 616 (1989).
[9] E. Fonda, F. Petroff, and A. Traverse, J. Appl. Phys. **93**, 5937 (2003).
[10] I. Arčon, M. Mozetič, A. Kodre, J. Jagielski, and A. Traverse, J. Synchrotron Radiat. **8**, 493 (2001).
[11] J. Lekner, *Theory of Reflection of Electromagnetic and Particle Waves* (Martinus Nijhoff, Dordrecht, 1987).
[12] H. Zabel, in Festköerperprobleme (Advances in Solid State Physics), edited by U. Rössler (Vieweg, Braunschweig, 1990), Vol. 30, p. 197; T. P. Russell, Annu. Rev. Mater. Sci. **21**, 249 (1991).
[13] S. K. Sinha, E. B. Sirota, S. Garoff, and H. B. Stanley, Phys. Rev. B **38**, 2297 (1988).
[14] S. J. Blundell and J. A. C. Bland, Phys. Rev. B **46**, 3391 (1992).
[15] C. F. Majkrzak, Physica B **173**, 75 (1991).
[16] R. W. Bené, Appl. Phys. Lett. **41**, 529 (1982).
[17] C. F. Majkrzak, Physica B **221**, 342 (1996).
[18] J. F. Ankner, C. F. Majkrzak, and H. Homma, J. Appl. Phys. **73**, 6436 (1993).
[19] S. Singh, S. Basu, P. Bhatt, and A. K. Poswal, Phys. Rev. B **79**, 195435 (2009).
[20] S. Singh and S. Basu, Solid State Physics, edited by S. L. Chaplot, P. S. R. Krishna, and T. Sakuntala (Narosa Publishing House, New Delhi, 2001), Vol. 44, p. 257.
[21] S. Singh, S. Basu, M. Gupta, M. Vedpathak, and R. H. Kodama, J. Appl. Phys. **101**, 033913 (2007).
[22] M. Chakraborty, A. Mookerjee, and A. K. Bhattacharya, J. Magn. Magn. Mater. **285**, 210 (2005).
[23] J. Speakman, P. Rose, J. A. Hunt, N. Cowlam, R. E. Somekh, and A. L. Greer, J. Magn. Magn. Mater. **156**, 411 (1996).